**EURASIP Journal on
Advances in Signal Processing**
a SpringerOpen Journal

RESEARCH   Open Access

Segmentation algorithm via Cellular Neural/ Nonlinear Network: implementation on Bio-inspired hardware platform

Fethullah Karabiber[1], Pietro Vecchio[2] and Giuseppe Grassi[2*]

Abstract

The Bio-inspired (Bi-i) Cellular Vision System is a computing platform consisting of sensing, array sensing-processing, and digital signal processing. The platform is based on the Cellular Neural/Nonlinear Network (CNN) paradigm. This article presents the implementation of a novel CNN-based segmentation algorithm onto the Bi-i system. Each part of the algorithm, along with the corresponding implementation on the hardware platform, is carefully described through the article. The experimental results, carried out for *Foreman* and *Car-phone* video sequences, highlight the feasibility of the approach, which provides a frame rate of about 26 frames/s. Comparisons with existing CNN-based methods show that the conceived approach is more accurate, thus representing a good trade-off between real-time requirements and accuracy.

Keywords: Cellular Neural/Nonlinear Networks, image segmentation, Bio-inspired hardware platform

1. Introduction

Due to the recent advances in communication technologies, the interest in video contents has increased significantly, and it has become more and more important to automatically analyze and understand video contents using computer vision techniques. In this regard, segmentation is essentially the first step toward many image analysis and computer vision problems [1-15]. With the recent advances in several new multimedia applications, there is the need to develop segmentation algorithms running on efficient hardware platforms [16-18]. To this purpose, in [16] an algorithm for the real-time segmentation of endoscopic images running on a special-purpose hardware architecture is described. The architecture detects the gastrointestinal lumen regions and generates binary segmented regions. In [17], a segmentation algorithm was proposed, along with the corresponding hardware architecture, mainly based on a connected component analysis of the binary difference image. In [18], a multiple-features neural-network-based segmentation algorithm and its hardware implementation have

been proposed. The algorithm incorporates static and dynamic features simultaneously in one scheme for segmenting a frame in an image sequence.

Referring to the development of segmentation algorithms running on hardware platforms, in this article the attention is focused on the implementation of algorithms running on the Cellular Neural/Nonlinear Network (CNN) Universal Machine [5-7]. This architecture offers great computational capabilities, which are suitable for complex image-analysis operations in object-oriented approaches [8-10]. Note that so far few CNN algorithms for obtaining the segmentation of a video sequence into moving objects have been introduced [5,6]. These segmentation algorithms were only simulated, i.e., the hardware implementation of these algorithms is substantially lacking. Based on these considerations, this article presents the implementation of a novel CNN-based segmentation algorithm onto the Bio-inspired (Bi-i) Cellular Vision System [9]. This system builds on CNN type (ACE16k) and DSP type (TX 6×) microprocessors [9]. The proposed segmentation approach focuses on the algorithmic issues of the Bi-i platform, rather than on the architectural ones. This algorithmic approach has been conceived with the aim of fully exploiting both the capabilities offered by the

* Correspondence: giuseppe.grassi@unisalento.it
[2]Dipartimento di Ingegneria dell'Innovazione, Università del Salento, 73100 Lecce, Italy
Full list of author information is available at the end of the article

Springer

Bi-i system, that is, the *analog* processing based on the ACE16k as well as the *digital* processing based on the DSP. We would point out that, referring to the segmentation process, the goal of our approach is to find moving objects in video sequences characterized by almost static background. We do not consider in this article still images or moving objects in a video captured by a camera located on a moving platform, where the background is also moving.

The article is organized as follows. Section 2 briefly revises the basic notions on the CNN model and the Bi-i cellular vision architecture. Then the segmentation algorithm is described in detail (see the block diagram in Figure 1). In particular, in Section 3, the motion detection is described, whereas Section 4 presents the edge detection phase, which consists of two blocks, the preliminary edge detection and the final edge detection. In Section 5, the object detection block is illustrated. All the algorithms are described from the point of view of their implementation on the Bi-i, that is, for each task it is specified which templates (of the CNN) run on the ACE16k chip and which parts run on the DSP. Finally, Section 6 reports comparisons between the proposed approach and the segmentation algorithms described in [3] and [5], which have been also implemented on the Bi-i Cellular Vision System.

2. Cellular Neural/Nonlinear Networks and Bio-Inspired Cellular Vision System

Cellular Neural/Nonlinear Networks represent an information processing system described by nonlinear ordinary differential equations (ODEs). These networks, which are composed of a large number of locally connected analog processing elements (called cells), are described by the following set of ODEs [1]:

$$\dot{x}_{ij}(t) = -x_{ij}(t) + \sum_{kl \in N_{\bar{r}}} A_{ij,kl} y_{kl}(t) + \sum_{kl \in N_{\bar{r}}} B_{ij,kl} u_{kl}(t) + I_{ij} \quad (1)$$
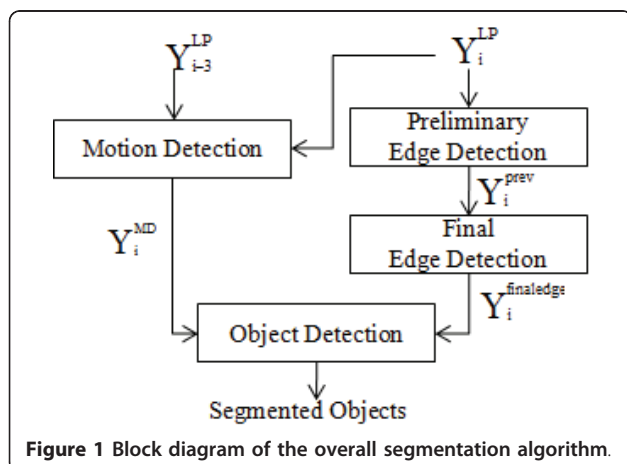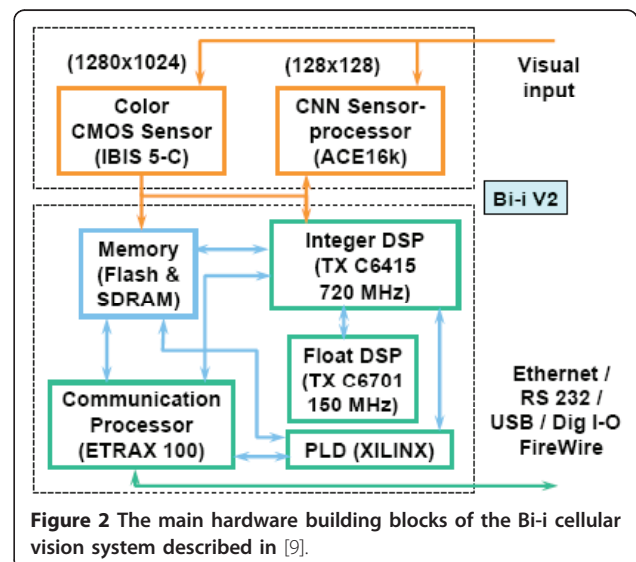
$$y_{ij}(t) = f(x_{ij}(t)) = 0.5 \left(\left| x_{ij}(t) + 1 \right| - \left| x_{ij}(t) - 1 \right| \right) \quad (2)$$

where $x_{ij}(t)$ is the state, $y_{ij}(t)$ the output, and $u_{ij}(t)$ the input. The constant I_{ij} is the cell current, which could also be interpreted as a space-varying threshold [19]. Moreover, $A_{ij,kl}$ and $B_{ij,kl}$ are the parameters forming the feedback template A and the control template B, respectively, whereas $kl \in N_{\bar{r}}$ is a grid point in the neighborhood within the radius $\bar{r}$ of the cell ij [20].

Since the cells cooperate in order to solve a given computational task, CNNs have provided in recent years an ideal framework for programmable analog array computing, where the instructions are represented by the templates. This is in fact the basic idea underlying the CNN Universal Machine [1], where the architecture combines analog array operations with logic operations (therefore named as *analogic* computing). A global programming unit was included in the architecture, along with the integration of an array of sensors. Moreover, local memories were added to each computing cell [1]. The physical implementations of the CNN Universal Machine with integrated sensor array proved the physical feasibility of the architecture [11,12].

Recently, a Bio-inspired (Bi-i) Cellular Vision System has been introduced, which combines Analogic Cellular Engine (ACE16k) and DSP type microprocessors [9]. Its algorithmic framework contains several feedback and automatic control mechanisms among the different processing stages [9]. In particular, this article exploits the Bi-i Version 2 (V2), which has been described in detail in reference [9]. The main hardware building blocks of this Bi-i architecture are illustrated in Figure 2. It has a color (1280 * 1024) CMOS sensor array (IBIS 5-C), two high-end digital signal processors (TX C6415 and TX

Figure 1 Block diagram of the overall segmentation algorithm.

Figure 2 The main hardware building blocks of the Bi-i cellular vision system described in [9].

C6701), and a communication processor (ETRAX 100) with some external interfaces (USB, FireWire, and a general digital I/O, in addition to the Ethernet and RS232).

Referring to the Analogic Cellular Engine ACE16k, note that a full description can be found in [12]. Herein, we recall that it represents a low resolution (128 * 128) grayscale image sensor array processor. Thus, the Bi-i is a reconfigurable device, i.e., it can be used as a monocular or a binocular device with a proper selection of a high-resolution CMOS sensor (IBIS 5-C) and a low-resolution CNN sensor processor (ACE16k) [9].

Two tools can be used in order to program the Bi-i Vision System, i.e., the analogic macro code (AMC) and the software development kit (SDK). In particular, by using the AMC language, the Bi-i Vision System can be programmed for simple analogic routines [9], whereas the SDK is used to design more complex algorithms (see Appendix). Referring to the image processing library (IPL), note that the so-called TACE_IPL is a library developed within the SDK. It contains useful functions for morphological and grey-scale processing in the ACE16k chip (see Appendix). Additionally, the Bi-i V2 includes an InstantVision™ library [9].

Finally, note that through the article, the attention is focused on the way the proposed segmentation algorithm is implemented onto the Bi-i Cellular Vision System. Namely, each step of the algorithm has been conceived with the aim of fully exploiting the Bi-i capabilities, i.e., the processing based on the ACE16k chip as well as the processing based on the DSP.

3. Motion detection

This section illustrates the *motion detection* algorithm (Figure 1). Let Y_i^{LP} and Y_{i-3}^{LP} be two gray-level images, processed by a low-pass (LP) filtering, and let Y_i^{MD} be the motion detection (MD) mask. In order to implement the *motion detection* onto the Bi-i, the first step (see Equation 3) consists in computing the *difference* between the current frame Y_i^{LP} and the third preceding frame Y_{i-3}^{LP} using the ACE16k chip. The indices i and i-3 denote that the frames i-2 and i-1 are skipped. Namely, the analysis of the video sequences considered through the article suggests that it is not necessary to compute the difference between successive frames, but it is enough every three frames. However, as far as the algorithm goes, every frame is evaluated, even though the reference frame is three frames older. This means that we need to store every frame, because the frame i + 1 requires frame i-2 as a reference.

Then, according to Step 2 in Equation 3, positive and negative *threshold* operations are applied to the

difference image via the *ConvLAMtoLLM* function [13] implemented on the ACE16k chip. This function (included in the SDK) converts a grey-level image stored in the local analog memory (LAM) into a binary image stored in the local logic memory (LLM). Successively, the logic OR operation is applied between the output of the positive threshold and the output of the negative threshold. The resulting image includes all the changed pixels.

$$
\begin{aligned}
&\text{step } 1 - \text{compute the difference between the frames } Y_i^{\mathrm{LP}} \text{ and } Y_{i-3}^{\mathrm{LP}} \\
&\text{step } 2 - \text{apply a positive and negative threshold} \\
&\text{step } 3 - \text{delete irrelevent pixel}
\end{aligned}
\tag{3}
$$

Finally, according to Step 3, the *Point Remove function* [13] (running on the ACE16k) is used for deleting irrelevant pixels not belonging to the contour lines. The output of the algorithm is the MD mask Y_i^{MD}, which entirely preserves the moving objects. Figure 3a, c shows a sample frame of *Foreman* and *Car-phone* video sequences, respectively, whereas Figure 3b, d shows the corresponding motion detection mask Y_i^{MD}.

4. Edge detection

The proposed *edge detection* phase consists of two blocks, the *preliminary edge detection* and the *final edge detection* (see Figure 1). In the first block, the CNN-
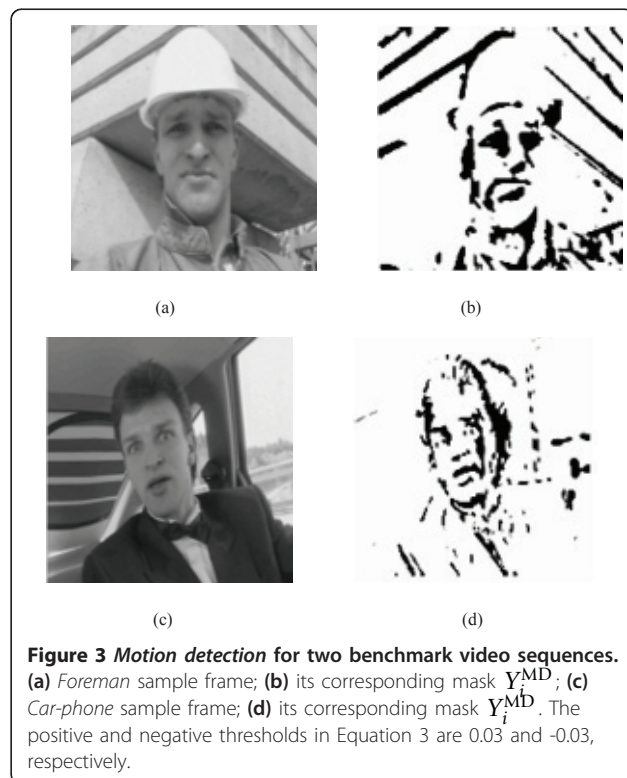
Figure 3 Motion detection for two benchmark video sequences. (a) *Foreman* sample frame; (b) its corresponding mask Y_i^{MD}; (c) *Car-phone* sample frame; (d) its corresponding mask Y_i^{MD}. The positive and negative thresholds in Equation 3 are 0.03 and -0.03, respectively.

based dual window operator (proposed by Grassi and Vecchio [10]) is exploited to reveal edges as zero-crossing points of a difference function, depending on the minimum and maximum values in the two windows. After this preliminary selection of edge candidates, the second block enables accurate edge detection to be obtained, using a technique able to highlight the discontinuity areas.

4.1. Preliminary edge detection

The aim of this phase is to locate the edge candidates. The dual window operator is based on a criterion able to localize the mean point within the transition area between two uniform luminance areas [10]. Thus, the first step consists in determining the minimum and maximum values in the two considered windows. Given the input image Y_i^{LP}, we consider for each sample $s \in Y_i^{\mathrm{LP}}(x, y)$ two concentric circular windows, centered in s and having radius r and R, respectively ($r < R$). Let M^R and m^R be the maximum and minimum values of Y_i^{LP} within the window of radius R, and let M^r and m^r be the maximum and minimum values within the window of radius r [10]. Note that, for the video-sequences considered through the article, we have taken the values $r = 1$ pixel and $R = 2$ pixels. For each sample s, let us define the difference function $D(s) = \alpha_1(s) - \alpha_2(s)$, where $\alpha_1(s) = M^R - M^r$ and $\alpha_2(s) = m^r - m^R$. By assuming that s is the middle point in a luminance transition, the relationship $\alpha_1(s) = \alpha_2(s)$ holds. In the case of noise, the change in the sign of the difference function $D(s)$ is a more effective indicator of the presence of a contour [10]. Since $D(s)$ approximates the directional derivative of the luminance signal along the gradient direction [10], the relationship $D(s) = 0$ is equivalent to find the flex points of luminance transitions. In particular, we look for zero-points and zero-crossing points of $D(s)$. Hence, the introduction of a threshold is required, so that samples s satisfy the condition -threshold $< D(s)$ <threshold. Successively, edge samples are detected according to the following algorithm [10]:

$$
\begin{aligned}
&\mathrm{step}\,1 - \mathrm{compute}\, D(s) = \alpha_1(s) - \alpha_2(s)\\
&\mathrm{step}\,2 - \mathrm{for\,each}\, s = (x_0,\, y_0)\, \mathrm{so\, that} - \mathrm{threshold}\; < D(s) < \mathrm{threshold}\\
&\qquad \mathrm{if}\, D(s) = 0\, \mathrm{then}\, s\, \mathrm{is\, edge}\\
&\qquad \mathrm{else\, if}\, D(s) \geq 0\, \mathrm{and}\, \binom{D(x_0-1, y_0) < 0\, \mathrm{or}\, D(x_0+1, y_0) < 0}{\mathrm{or}\, D(x_0, y_0-1) < 0\, \mathrm{or}\, D(x_0, y_0+1) < 0}\, \mathrm{then}\, s\, \mathrm{is\, edge.}
\end{aligned}
\tag{4}
$$

In other words, by applying the algorithm (4) to the sample itself and to the four neighboring samples, preliminary edge detection is achieved. In order to effectively implement (4) onto the Bi-i, the first step is the computation of $D(s)$, which can be realized using order-statistics filters. They are nonlinear spatial filters that enable maximum and minimum values to be readily computed onto the Bi-i platform. Their behaviors consist in ordering the pixels contained in a neighborhood of the current pixel, and then replacing the pixel in the centre of the neighborhood with the value determined by the selected method. Therefore, these filters are well suited to find the minimum and maximum values in the neighborhood of the current pixel. The implementation of D(s) gives the images in Figure 4a, c for *Foreman* and *Car-phone*, respectively.

Going to Step 2, the *threshold* is implemented on the ACE16k using the *ConvLAMtoLLM* function. Then, the relationship -threshold $< D(s)$ <threshold is satisfied by implementing the operations *inversion*, OR and *inversion* again onto the ACE16k chip. Note that we look for samples s so that $D(s) = 0$. Additionally, we look for samples s satisfying the condition that $D(s) \geq 0$ but, simultaneously, $D(s)$ must be negative in a cross-shape neighborhood of s. Specifically, at least one of the four conditions $D(x_0 \pm 1, y_0 \pm 1) < 0$ must be satisfied. Thus, we need to compute D(s) by exploring proper neighborhoods of (x_0, y_0), two examples of which are reported in Figure 4e, f. Note that the object is represented by black pixels, while the background is represented by white pixels. The exploration of proper neighborhoods in the image D(s) can be done using the morphologic *dilate4* function, which performs four-connectivity (cross-mask) binary dilation on the ACE16k [13]. Note that Figure 4e contains an edge, since the conditions $D(x_0-1, y_0) < 0$ and $D(x_0, y_0-1) < 0$ are satisfied. On the other hand, Figure 4f does not contain any edge, since $D(s) > 0$ in the neighborhood of (x_0, y_0). Referring to *Foreman*, the edges selected by implementing the condition -threshold $< D(s)$ <threshold are reported in Figure 4g, whereas those selected by exploring proper neighborhoods of (x_0, y_0) are reported in Figure 4h. In particular, note that Figure 4h highlights that there are some flat areas characterized by some edges. Finally, the OR operation between the images in Figure 4g, h provides the image Y_i^{prel} representing the preliminary edge detection. To this purpose, Figure 4b, d depicts the images Y_i^{prel} for *Foreman* and *Car-phone* video sequences, respectively.

4.2. Final edge detection

The aim of this phase is to better select the previously detected edges. Referring to the previous section, note that the zeros of $D(s)$ are not only flex points of luminance transitions, but also the set of pixels having a neighborhood where luminance is almost constant [10]. Since noise causes small fluctuations, these fluctuations may generate changes in the sign of D that would be incorrectly assumed as edge points. Therefore, in order to better select the edges detected in the previous phase, we need to integrate the available information with the slope of the luminance signal. To this purpose, note that
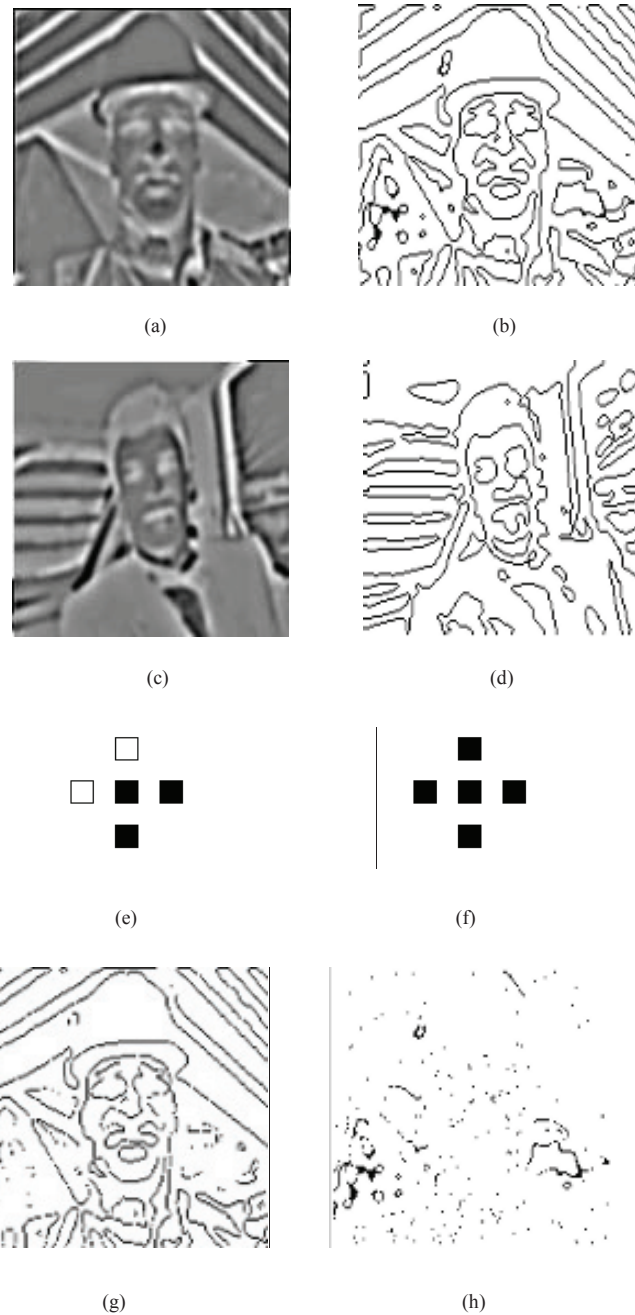
Figure 4 *Preliminary edge detection* algorithm.(a) matrix **D**(s) for *Foreman*; **(b)** corresponding outcome Y_i^{prel}; **(c)** matrix **D**(s) for *Car-phone*; **(d)** corresponding outcome Y_i^{prel}; **(e)** neighborhood of (x_0, y_0) containing and edge; **(f)** neighborhood of (x_0, y_0) not containing any edge; **(g)** edges obtained by the condition -threshold <**D**(s) <threshold; **(h)** edges obtained by the four conditions on the neighborhoods of (x_0, y_0).

M^R and m^R identify the direction of maximum slope in the neighborhood of s [10]. Therefore, by suitably exploiting M^R and m^R, we first need to generate a matrix **S**, which takes into account the *slope* of the luminance signal. Then, a *threshold gradient* operation is applied to **S**, with the aim to obtain a *gradient* matrix

G. Namely, the final objective is to obtain an image that includes all the edges selected by the gradient operation (i.e., Y_i^{grad}). Successively, the image Y_i^{grad} needs to be cleaned and skeletonized, in order to reduce all the edges to one-pixel thin lines. The image reporting the

final edge detection, indicated by $Y_i^{\text{final edge}}(s)$, can be obtained by applying the following algorithm:

$$\text{step 1} - \text{for each pixel } s = (x_0, y_0) \in D \text{ compute } s(s) = \left\{ \begin{array}{l} M^R(s) \text{ if } D(s) \geq 0 \\ m^R(s) \text{ if } D(s) < 0 \end{array} \right\}$$

$$\text{step 2} - \text{apply a } \textit{threshold gradient} \text{ operation on } S(s) \text{ to obtain } G(s)$$

$$\text{step 3} - \text{for each pixel } s \in Y_i^{pre1}(s) \text{ compute } Y_i^{grad}(s) = \left\{ \begin{array}{l} Y_i^{pre1}(s) \text{ if } s \in G(s) \\ \emptyset \text{ if } s \notin G(s) \end{array} \right. \quad (5)$$

$$\text{step 4} - \text{skeletonize } Y_i^{grad}(s) \text{ to obtain } Y_i^{final\,edge}(s)$$

In order to effectively implement the algorithm (5) onto the Bi-i, at first the matrix $D(s)$ is processed by means of the *ConvLAMtoLLM* function, which implements the threshold 'zero' on $D(s)$. Then, the pixels in D that correspond to $D(s) \geq 0$ assume the maximum value of the luminance signal (within the window of radius R) and generate the image M_D^R. Similarly, the pixels in D that correspond to $D(s) < 0$ assume the minimum value of the luminance signal and generate the image m_D^R. Then, in order to implement the matrix $S(s)$, we need the following new *switch* template:

$$A = \begin{bmatrix} 0 & 0 & 0 \\ 0 & -1 & 0 \\ 0 & 0 & 0 \end{bmatrix} \quad B = \begin{bmatrix} 0 & 0 & 0 \\ 0 & 2.2 & 0 \\ 0 & 0 & 0 \end{bmatrix} \quad I = 0 \quad (6)$$

The matrix $S(s)$ is generated onto the ACE16k chip, where M_D^R is used as *input*, m_D^R as *state* whereas the output of the 'zero' threshold is used as *mask*. Referring to the template (6), we have chosen the name *switch* since the image $S(s)$ is obtained by 'switching' between $M^R(s)$ and $m^R(s)$, depending on the mask values. Note that the template (6), by providing the matrix $S(s)$, enables the *slope* of the luminance signal to be taken into account. The experimental result of $S(s)$ are reported in Figures 5a and 6a for *Foreman* and *Carphone*, respectively.

Then, according to the algorithm (5), we need to implement the *threshold gradient* operation onto the Bi-i. This can be done using a sequence of eight templates, applied in eight directions N, NW, NE, W, E, SW, S, and SE. For example, referring to the NW direction, the following novel template is implemented on the ACE16k:

$$A = \begin{bmatrix} 0 & 0 & 0 \\ 0 & 1 & 0 \\ 0 & 0 & 0 \end{bmatrix} \quad B = \begin{bmatrix} -3 & 0 & 0 \\ 0 & 3 & 0 \\ 0 & 0 & 0 \end{bmatrix} \quad I = \text{thres (NW)} \quad (7)$$

where the bias is used as a threshold level (herein, thres = -1.1). The other seven remaining templates can be easily derived from (7). Then the logic OR is applied
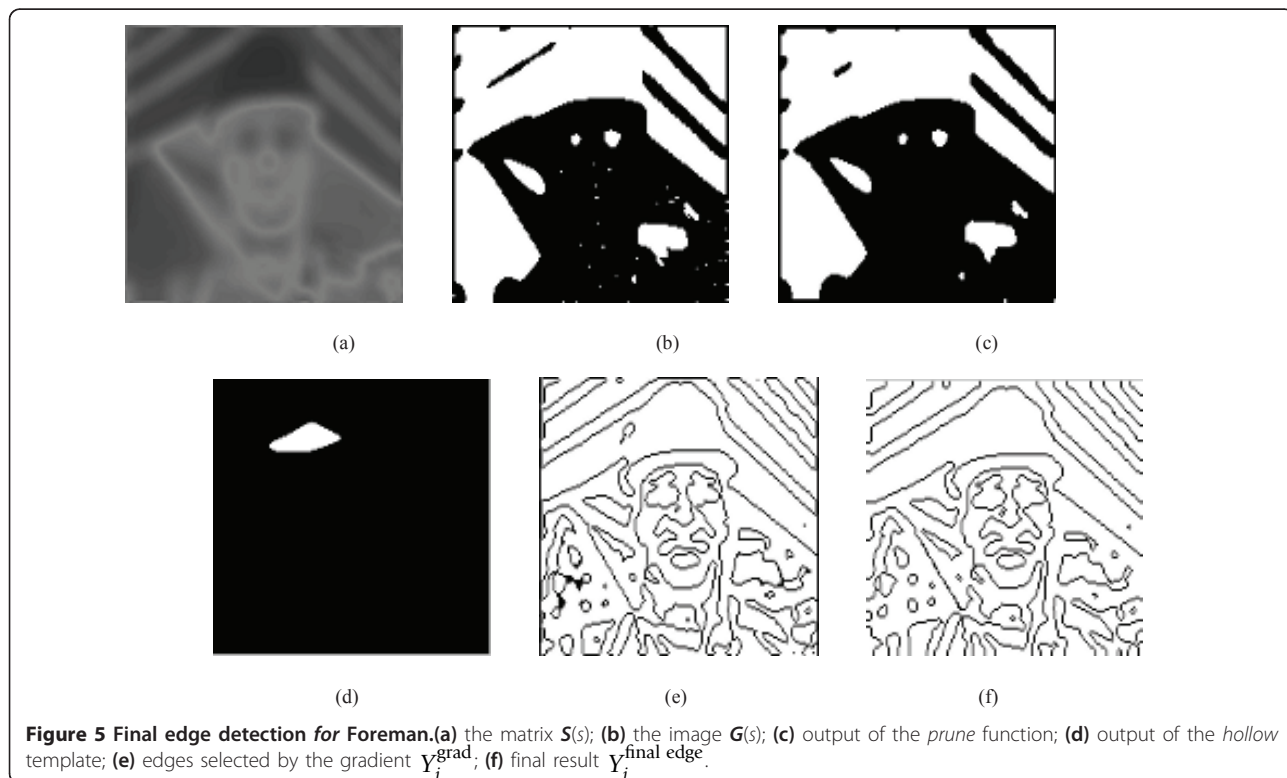
Figure 5 Final edge detection for Foreman. **(a)** the matrix $S(s)$; **(b)** the image $G(s)$; **(c)** output of the *prune* function; **(d)** output of the *hollow* template; **(e)** edges selected by the gradient Y_i^{grad}; **(f)** final result $Y_i^{\text{final edge}}$.
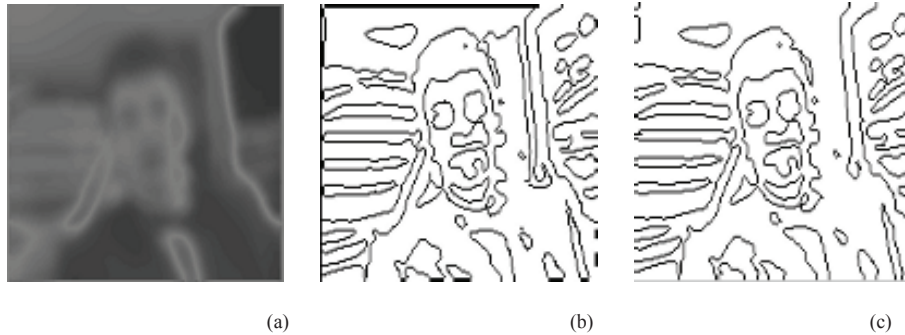
Figure 6 Final edge detection *for* Car-phone.(a) the matrix $S(s)$; **(b)** edges selected by the gradient Y_i^{grad}; **(c)** final result $Y_i^{\text{final edge}}$.

to the eight output images in order to obtain a single image, which is denoted by $G(s)$ (see Figure 5b). Note that G stands for *gradient*, given that it represents the output of the threshold gradient (7). However, the image G needs to be cleaned, since it usually contains some open lines (see the upper left-side in Figure 5b). These open lines can be deleted by applying the *prune* template:

$$A = \begin{bmatrix} 0 & 0.5 & 0 \\ 0.5 & 3 & 0.5 \\ 0 & 0.5 & 0 \end{bmatrix} \quad B = \begin{bmatrix} 0 & 0 & 0 \\ 0 & 0 & 0 \\ 0 & 0 & 0 \end{bmatrix} \quad I = -1.5. \tag{8}$$

The output of the *prune* function is reported in Figure 5c, where it can be seen that the open line in the upper left-side part has been partially deleted. Note that the *prune* function also enables the back part in Figure 5c to become more compact (i.e., the white dots in the black part have disappeared). Then, the *hollow* template reported in [13] has to be applied. This template, running on the ACE16k chip, enables the concave locations of objects to be filled. In order to achieve this objective, the *hollow* template needs to be applied. The output of the *hollow* is shown in Figure 5d. The white part in Figure 5d indicates that the corresponding part in the image $S(s)$ does not contain information related to edges. Since the hollow is time-consuming, it is useful to carry out this operation by exploiting the great computational power offered by the CNN chip.

Finally, by using the *switch* template (6) with input = $Y_i^{\text{prel}}(s)$, state = $\varnothing$ (i.e., the white image) and mask = $G(s)$, it is possible to obtain the image $Y_i^{\text{grad}}(s)$, which includes all the edges selected by the gradient operation (see Figures 5e and 6b). In order to skeletonize $Y_i^{\text{grad}}(s)$ and reduce all the edges to one-pixel thin lines, the *skeletonization* function (included in the TACE_IPL library) is implemented on the ACE16k chip. Then, in order to complete open edges (if any) we can use the *dilation* and *erosion* functions included

in the TACE_IPL. Specifically, we first apply the *dilation* function, and then the *erosion* function. These two functions are applied from three to six times, depending on the video sequence under consideration. Finally, the last step lies in deleting the remaining open lines. By applying the *prune* template (8), the final edges can be obtained, as shown by the images $Y_i^{\text{final edge}}(s)$ reported in Figures 5f and 6c for *Foreman* and *Car-phone*, respectively.

5. Object detection

The proposed *object detection* phase can be described using the following iterative procedure:
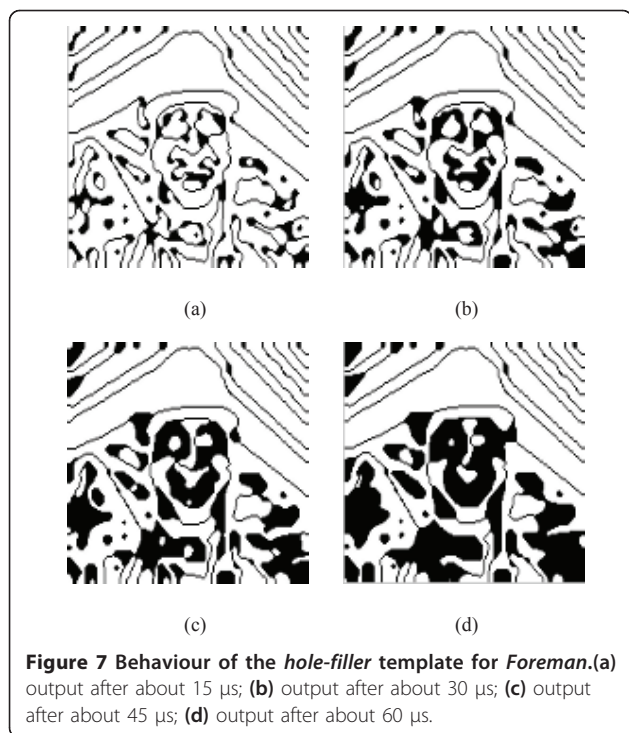
$$\begin{aligned}
&\text{BEGIN}: k = 1 \\
&\text{step 1} - - - \text{fill closed edges (notsimultaneously) in the inverted image of } Y_i^{\text{final edge}} \text{ to obtain } Y_i^{\text{fill}(k)} \\
&\text{step 2} - - - \text{detect changes between } Y_i^{\text{fill}(k)} \text{ and } (-Y_i^{\text{final edge}}) \text{ to obtain } Y_i^{\text{changes}(k)} \\
&\text{step 3} - - - \text{fill closed edges in } Y_i^{\text{fill}(k)} \text{ to obtain } Y_i^{\text{fill}(k+1)}. \\
&\text{step 4} - - - \text{thicken edges in } Y_i^{\text{fill}(k+1)} \text{ to obtain } Y_i^{\text{dilation}(k+1)}. \\
&\text{step 5} - - - \text{detect objects in } Y_i^{\text{dilation}(k+1)} \text{ to obtain } Y_i^{\text{recall}(k+1)} \\
&\text{step 6} - - - \text{detect changes between } Y_i^{\text{recall}(k+1)} \text{ and } Y_i^{\text{changes}(k)} \\
&\quad \text{if changes} \neq 0 \text{ and if the extracted object } Y_i^{\text{extracted}(k+1)} \text{ is a moving object,} \\
&\quad \text{then update } Y_i^{\text{changes}(k)} \\
&\text{step 7} - - - \text{assign } k = k + 1 \\
&\text{step 8} - - - \text{if } Y_i^{\text{fill}(k)} \neq Y_i^{\text{fill}(k+1)} \text{ go to step 3 else END}
\end{aligned} \tag{9}$$

First, the following *hole-filler* template is implemented on the ACE16k:

$$\mathbf{A} = \begin{bmatrix} 0.1 & 0.2 & 0.1 \\ 0.2 & 1 & 0.2 \\ 0.1 & 0.2 & 0.1 \end{bmatrix} \quad \mathbf{B} = \begin{bmatrix} 0 & 0 & 0 \\ 0 & 1 & 0 \\ 0 & 0 & 0 \end{bmatrix} \quad \mathbf{I} = 1.3. \tag{10}$$

This template is applied to the inverted image of $Y_i^{\text{final edge}}$ with the aim to fill all the holes. Figure 7 depicts the outputs of the *hole-filler* after different processing times, with the aim to show the system behavior when the processing times are increased. Note that the *hole-filler* has to be applied in a recursive way, in order to fill more and more holes. However, differently from Figure 7 that has an explanatory purpose, we need to apply this template by slowly increasing the processing

Figure 7 Behaviour of the *hole-filler* template for *Foreman*.(a) output after about 15 μs; **(b)** output after about 30 μs; **(c)** output after about 45 μs; **(d)** output after about 60 μs.

LLM1 and LLM2 (binary images stored in the Local Logic Memories 1 and 2). Herein, the outcome of the XOR is the binary image $Y_i^{\text{changes}\,(k)}$, which locates the changes between the two images $Y_i^{\text{fill}\,(k)}$ and $\left(-Y_i^{\text{final edge}}\right)$. The output of the XOR is shown in Figure 8a.

According to Step 3, the *hole-filler* template is applied to $Y_i^{\text{fill}\,(k)}$, with the aim to obtain $Y_i^{\text{fill}\,(k+1)}$. Referring to Step 4, the morphologic *dilate* function is utilized to thicken the contours within the image $Y_i^{\text{fill}\,(k+1)}$. The result of the *dilate* function, which performs binary dilatation onto the ACE16k, is indicated by $Y_i^{\text{dilation}\,(k+1)}$ and is shown in Figure 8b.

According to Step 5, we need to detect the remaining objects in $Y_i^{\text{dilation}\,(k+1)}$. This can be done using the *recall* template

$$
\mathbf{A} = \begin{bmatrix} 0.5 & 0.5 & 0.5 \\ 0.5 & 3 & 0.5 \\ 0.5 & 0.5 & 0.5 \end{bmatrix} \quad \mathbf{B} = \begin{bmatrix} 0 & 0 & 0 \\ 0 & 3 & 0 \\ 0 & 0 & 0 \end{bmatrix} \quad \mathbf{I} = 3 \qquad (11)
$$

where the image $Y_i^{\text{dilation}\,(k+1)}$ is used as *input* and the image $Y_i^{\text{final edge}}$ as *state*. In order to show how the *recall* template works, Figure 9 shows its output after different processing times. Note that the *recall* template has to be applied in a recursive way. In particular, by increasing the processing times, note that more and more objects are recalled (see Figure 9).

However, differently from Figure 9 that has an explanatory purpose, herein we need to apply this template by slowly increasing the processing times. Namely, in order to guarantee a satisfying total frame rate, we need to recall few objects at a time, so that the processing times due to the recall template are not large. In this way, the slow recursive application of the recall template
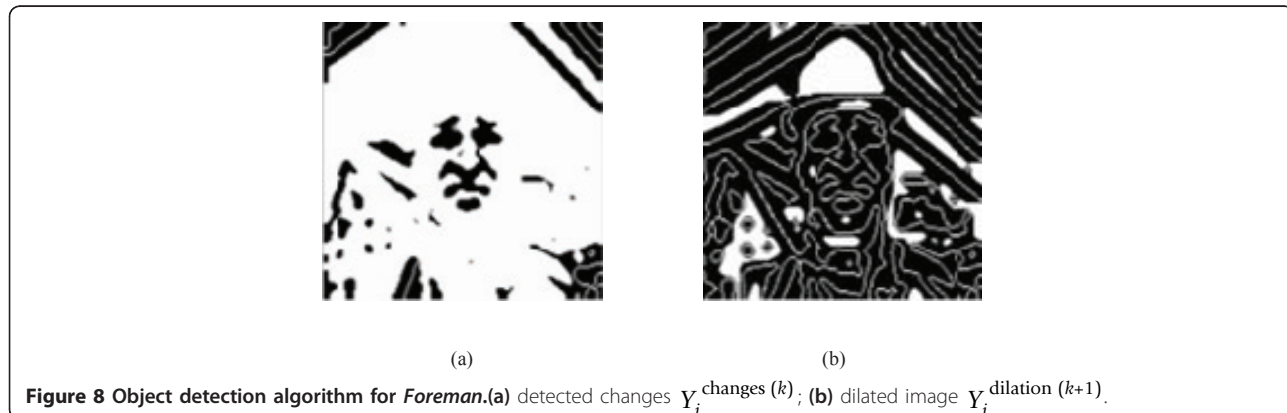
times. Namely, if we slowly increase the processing times, it is possible to highlight at the most two closed objects at a time, so that these objects can be extracted in the next steps. As a consequence, the *hole-filler* plays an important role: by slowly filling the holes in a morphological way, it enables the closed objects to be extracted in the next steps of the algorithm.

In order to implement the second step, the logic XOR is applied between the output of the *hole-filler* (i.e., $Y_i^{\text{fill}\,(k)}$) and the inverted image of $Y_i^{\text{final edge}}$. Note that the logic XOR enables changes in the two images to be detected. This logic function returns a 1 only if both operands are logically different, otherwise it returns a 0. Bitwise logic XOR is executed on the ACE16k between

Figure 8 Object detection algorithm for *Foreman*.(a) detected changes $Y_i^{\text{changes}\,(k)}$; **(b)** dilated image $Y_i^{\text{dilation}\,(k+1)}$.
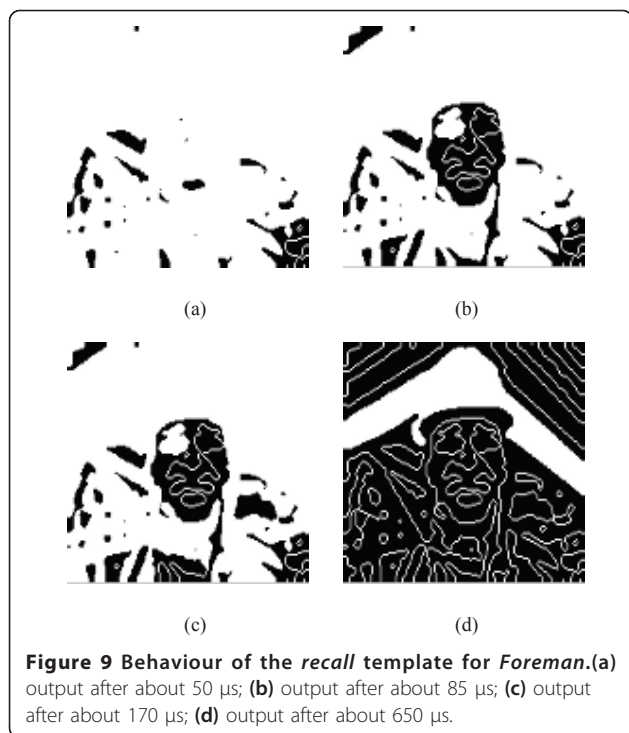
Figure 9 Behaviour of the *recall* template for *Foreman*.(a) output after about 50 μs; **(b)** output after about 85 μs; **(c)** output after about 170 μs; **(d)** output after about 650 μs.

does not affect the overall system performances. In conclusion, the recall template plays an important role: by taking into account the image containing the final edge (*state*), it enables the objects enclosed in the dilated image (*input*) to be recalled and subsequently extracted.

Now, by applying the recall template (11) using the image in Figure 8b as *input* and the image in Figure 5f as *state*, the image reported in Figure 10a is obtained. This image, indicated by $Y_i^{\text{recall}\,(k+1)}$, is constituted by groups of objects. In order to obtain new objects at each iteration, we need to detect the changes between the images $Y_i^{\text{recall}\,(k+1)}$ and $Y_i^{\text{changes}\,(k)}$, as indicated by Step 6. To this purpose, we can apply the logic XOR between

$Y_i^{\text{changes}\,(k)}$ and $Y_i^{\text{changes}\,(k)}$. If changes are detected, we need to check whether the extracted object belongs to the moving objects. This operation is implemented by exploiting the AND operation between the output of previous XOR and the motion detection mask Y_i^{MD}. The output of the AND is indicated by $Y_i^{\text{extracted}\,(k+1)}$. For example, the objects extracted after the first iteration are shown in Figure 10b. Finally, the extracted object $Y_i^{\text{extracted}\,(k+1)}$ is used to update the image $Y_i^{\text{changes}\,(k)}$, with the aim of obtaining $Y_i^{\text{changes}\,(k+1)}$. This iterative procedure is carried out until all the objects are extracted. Namely, the procedure ends when the condition $Y_i^{\text{fill}\,(k)} = Y_i^{\text{fill}\,(k+1)}$ is achieved for two consecutive iterations. Figures 8 and 10 summarize some of the fundamental steps of the *object detection* algorithm for *Foreman* video sequence. Similar results have been obtained for *Car-phone* video sequence.

6. Discussion

We discuss the results of our approach by making comparisons with previous CNN-based methods illustrated in [3] and [5]. We would remark that the comparison between the proposed approach and the methods in [3] and [5] is homogeneous, since we have implemented all these techniques on the same hardware platform (i.e., the Bi-i). At first, we compare these approaches by visual inspection. By analyzing the results in Figures 11 and 12, it can be noticed that the proposed technique provides more accurate segmented objects than the ones obtained by the techniques in [5] and [3]. For example, the analysis of Figure 11a suggests that the proposed approach is able to detect man's mouth, eyes, and nose. Note the absence of open lines too. The methods depicted in Figure 11b, c do not offer similar capabilities. Referring to Figure 12a, note that we have obtained an accurate result, since man's mouth, eyes, and nose
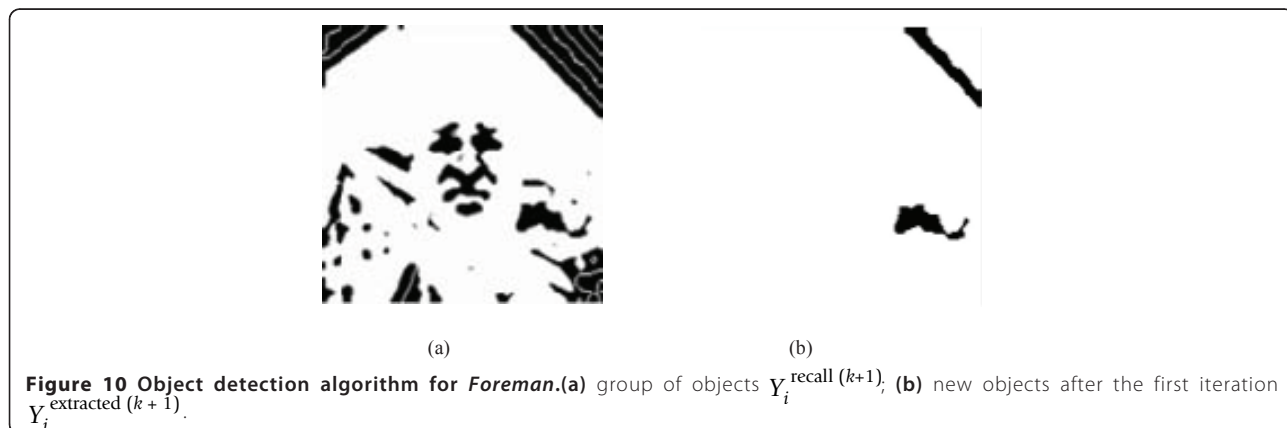
Figure 10 Object detection algorithm for *Foreman*.(a) group of objects $Y_i^{\text{recall}\,(k+1)}$; **(b)** new objects after the first iteration $Y_i^{\text{extracted}\,(k+1)}$.
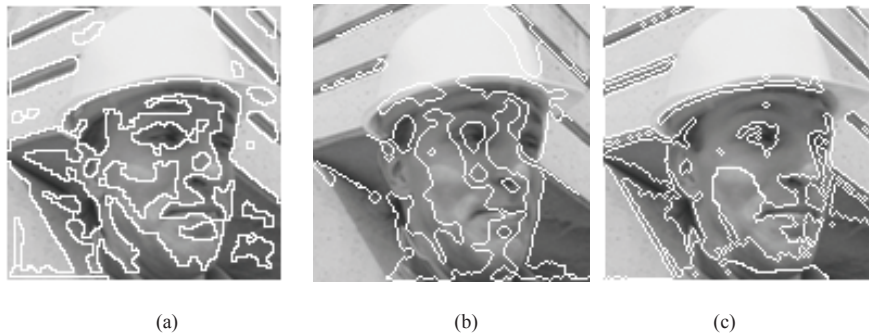
Figure 11 *Foreman* video sequence.(a) segmentation by our method; **(b)** segmentation by the method in [5]; **(c)** early segmentation in [3].

are detected, along with some moving parts in the back of the car. Again, the approaches depicted in Figure 12b, c do not reach similar performances. It can be concluded that, by exploiting the proposed approach, the edges are much more close to the real edges with respect to the method in [5] and [3].

Now an estimation of the processing time achievable by the proposed approach is given in Table 1. Note that the *motion detection* and the *object detection* phases can be fully implemented onto the ACE16k chip, whereas the *edge detection* phase requires that some parts be implemented on the DSP (see Section 4). The sum of the processing times of the different phases is 37767 μs, which gives a frame rate of about 26 frames/s.

Note that the computational load is mainly due to the DSP in the *edge detection* phase (28778 μs) and, specifically, to the presence of the order-statistics filters. On the other hand, these filters are requested to implement the dual window operator, which is in turn required to achieve accurate edge detection, as explained in [10]. Namely, edge detection is a crucial step for segmentation. If we detect edge accurately, we can segment the images correctly. If we analyze the result in reference [5], we note that the authors use a threshold gradient algorithm, which is not particularly suitable for edge detection. On the other hand,

the dual window operator is one of the best edge detector (see [10]), even though its implementation is time consuming. Referring to the processing times measured on the Bi-i for the methods in [3] and [5], their values are 13861 and 5254 μs, respectively. The corresponding frame rates are 72 and 190 frames/s, respectively, while our approach gives 26 frames/s. Thus, the segmentation methods in [3] and [5] are faster than the proposed approach, even though they are less accurate, as confirmed by Figures 11 and 12. Anyway, we believe that 26 frames/s can be considered a satisfying frame rate achievable by the proposed approach, since it represents a good trade-off between accuracy and speed.

Finally, we would point out that, while we have conducted this research, a novel Bio-inspired architecture called Eye-RIS vision system has been introduced [21]. It is based on the Q-Eye chip [21], which represents an evolution of the ACE family with the aim to overcome the main drawbacks of ACE chips, such as lack of robustness and large power consumption. Our plan is to implement the segmentation algorithm developed herein on the Eye-RIS vision system in the near future. To this purpose, note that one of the authors (F. Karabiber) has already started to work on the Eye-RIS vision system, as is proof by the results published in [22].
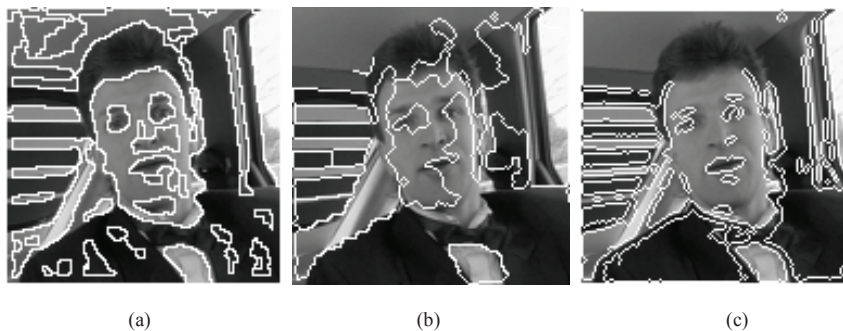
Figure 12 *Car-phone* video sequence.(a) segmentation by our method; **(b)** segmentation by the method in [5]; **(c)** early segmentation in [3].

Table 1 Execution times for the proposed segmentation algorithm

Motion detection	469 μs → (ACE16k)
Edge detection	34874 μs → 6096 μs (ACE16k) + 28778 μs (DSP)
Object detection	2424 μs → (ACE16K)
Total	37767 μs

7. Conclusion

This article has presented the implementation of a novel CNN-based segmentation algorithm onto a Bio-inspired hardware platform, called Bi-i Cellular Vision System [9]. This platform combines the *analog* processing based on the ACE16k processor [11] as well as the *digital* processing based on the DSP. The proposed experimental results, carried out for some benchmark video sequences, have shown the feasibility of the approach, which provides a satisfying frame rate of about 26 frames/s. Finally, comparisons with the CNN-based techniques in [5] and [3] have highlighted the accuracy of the proposed method.

Appendix

The software development kit (SDK) is a set of C++ libraries to be used for Bi-i programming. Some parts of the SDK are based on classes defined in the BaseData module of the InstantVision™ libraries. The SDK is designed to be used together with Code Composer Studio from Texas Instruments (http://www.ti.com/).

The TACE_IPL is an image processing library (IPL) for ACE16k. It contains two function groups for processing images: morphological operations and gray scale operations. The constructor of this class initializes the needed instruction group and writes corresponding IPL templates to the ACE16k.

Note that all the details about the SDK, the InstantVision™ libraries and the TACE_IPL can be found at: http://www.analogic-computers.com/Support/Documentation/

Alternatively, the Bi-i programming guide (which includes the SDK and the TACE_IPL) can be requested at: giuseppe.grassi@unisalento.it

List of abbreviations

AMC: Analogic Macro Code; Bi-i: Bio-inspired; CNN: Cellular Neural/Nonlinear Network; IPL: image processing library; LP: low pass; LAM: local analog memory; LLM: local logic memory; MD: motion detection; ODEs: ordinary differential equations; SDK: software development kit.

Author details

¹Department of Chemistry, University of North Carolina, Chapel Hill, NC, 27599-3290, USA ²Dipartimento di Ingegneria dell'Innovazione, Università del Salento, 73100 Lecce, Italy

Competing interests

The authors declare that they have no competing interests.

References

1. LO Chua, T Roska, in *Cellular Neural Networks and Visual Computing– Foundations and Applications* ((Cambridge University Press, 2002), Cambridge, UK), ISBN 0521652472
2. C-Y Chen, J-C Wang, J-F Wang, Y-H Hu, motion entropy feature and its applications to event-based segmentation of sports video. EURASIP J Adv Signal Process. **2008**(8) (2008). (Article ID 460913)
3. P Arena, A Basile, M Bucolo, L Fortuna, An object-oriented segmentation on analog CNN chip. IEEE Trans CAS-I **50**(7), 837–846 (2003). doi:10.1109/TCSI.2003.813985
4. MAA Dewan, MJ Hossain, O Chae, An adaptive motion segmentation for automated video surveillance. EURASIP J Adv Signal Process. **2008**(13) (2008). (Article ID 187413)
5. A Stoffels, T Roska, LO Chua, Object-oriented image analysis for very-low-bitrate video-coding systems using the CNN Universal Machine. Int J Circuit Theory Appl. **25**, 235–258 (1997). doi:10.1002/(SICI)1097-007X(199707/08)25:43.0.CO;2-Q
6. A Stoffels, T Roska, LO Chua, On object-oriented video-coding using the CNN Universal Machine. IEEE Trans CAS-I, **43**(11), 948–952 (1996)
7. T Roska, A Rodriguez-Vazquez, Towards visual microprocessors. Proc IEEE. **90**(7), 1244–1257 (2002). doi:10.1109/JPROC.2002.801453
8. G Grassi, LA Grieco, Object-oriented image analysis using the CNN Universal Machine: new analogic CNN algorithms for motion compensation, image synthesis and consistency observation. IEEE Trans CAS-I. **50**(4), 488–499 (2003). doi:10.1109/TCSI.2003.809812
9. A Zarandy, C Rekeczky, Bi-i: a standalone ultra high speed cellular vision system. IEEE Circuit Syst Mag. **5**(2), 36–45 (2005)
10. G Grassi, E Di Sciascio, LA Grieco, P Vecchio, New object-oriented segmentation algorithm based on the CNN paradigm. IEEE Trans CAS-II. **53**(4), 259–263 (2006)
11. G Linan, S Espejo, R Dominguez-Castro, A Rodriguez-Vazquez, ACE4k: an analog I/O 64x64 visual microprocessor chip with 7-bit analog accuracy. Int J Circuit Theory Appl, 30, 89–116 (2002)
12. A Rodriguez-Vazquez, G Linan-Cembrano, L Carranza, E Roca-Moreno, R Carmona-Galan, F Jimenez-Garrido, R Dominguez-Castro, SE Meana, ACE16k: the third generation of mixed-signal SIMDCNN ACE chips toward VSoCs. IEEE Trans CAS-I **51**(5), 851–863 (2004). doi:10.1109/TCSI.2004.827621
13. http://cnn-technology.itk.ppke.hu/
14. J-K Ahn, D-Y Lee, C Lee, C-S Kim, Automatic moving object segmentation from video sequences using alternate flashing system. EURASIP J Adv Signal Process. **2010** (14). (Article ID 340717)
15. C-Y Hsu, C-H Yang, H-C Wang, Multi-threshold level set model for image segmentation. EURASIP J Adv Signal Process. **2010**(8) (2010). (Article ID 950438)
16. J Kim, T Chen, A VLSI architecture for video-object segmentation. IEEE Trans CAS Video Technol. **13**(1), 83–96 (2003). doi:10.1109/TCSVT.2002.808082
17. N Ranganathan, R Mehrotra, A VLSI architecture for dynamic scene analysis. Comp Vis Graph Image Process. 5, 189–197 (1991)
18. J Kim, T Chen, Multiple feature clustering for image sequence segmentation. Pattern Recog Lett. 22, 1207–1217 (2001). doi:10.1016/S0167-8655(01)00053-8
19. M Brucoli, L Carnimeo, G Grassi, A global approach to the design of discrete-time cellular neural networks for associative memories. Int J Circuit Theory Appl. **24**(4), 489–510 (1996). doi:10.1002/(SICI)1097-007X(199607/08)24:43.0.CO;2-F
20. G Grassi, On discrete-time cellular neural networks for associative memories. IEEE Trans CAS-I, **48**(1), 107–111 (2001). doi:10.1109/81.903193
21. A Rodríguez-Vázquez, R Domínguez-Castro, F Jiménez-Garrido, S Morillas, J Listán, L Alba, G Liñán-Cembrano, L Carranza, The Eye-RIS CMOS vision system, in *Analog Circuit Design*, (Berlin, Germany, 2007), pp. 15–32
22. F Karabiber, P Arena, L Fortuna, S De Fiore, S Vagliasindi, S Arik, Implementation of a moving target tracking algorithm using Eye-RIS Vision System on a mobile robot. J Signal Process Syst (2010)